ESAIM: PROCEEDINGS AND SURVEYS, Vol. ?, 2019, 1-10
Editors: Will be set by the publisher

GEOMETRY DESCRIPTION AND MESH CONSTRUCTION FROM MEDICAL IMAGING

Michele Giuliano Carlino[1], Philippe Ricka[2], Minh Phan[3], Silvia Bertoluzza[4], Micol Pennacchio[4], Giuseppe Patanè[4] and Michela Spagnuolo[4]

Abstract. We present a new method for defining and meshing patient-specific domains from medical images. Our approach is based on an atlas image segmentation technique, and relies on the modular registration algorithm of S. Bertoluzza *et al.* [22]. The mesh of the patient-specific domain is generated by deforming the corresponding meshe on an a priori segmented and meshed reference image (the atlas). Our method aims at automating the process at the interface of medical imaging and numerical simulation, thus reducing the computational cost in those situations where simulations have to be managed on numerous medical images of similar patients.

Résumé. Nous présentons une nouvelle méthode de reconnaissance et de maillage d'un domaine d'intérêt d'une image médicale. Notre approche se base sur la méthode de segmentation à partir d'un atlas, et dépend de la boîte à outils modulaire pour la co-registration d'images développée par S. Bertoluzza *et al.* [22]. Le maillage du domaine spécifique au patient est généré par déformation du maillage correspondent sur une image de référence segmenté a priori (l'atlas). Notre Method vise à automatiser le processus à linterface entre l'imagerie médicale et la simulation numérique, avec le but de réduire le coût computationnel dans les situations dans lesquelles des simulations doivent être faites sur des nombreuses images similaires.

Introduction

The need for mathematical modeling and numerical simulation of patient-specific biophysical phenomena is becoming an essential medical demand in the real life. The mathematical modeling and numerical simulation of biophysical phaenomena relying on patient-specific data is nowadays recognized as an important step in the diagnosis of diseases and design of personalized treatment, and the demand for increasingly efficient tools for carrying out such tasks is attracting the interest of an ever increasing number of researchers. In this framework, whatever the application considered, one of the first key steps is to retrieve, often from a medical image, the geometrical description of the domain corresponding to the organ of interest on which the simulation will be run (called *patient-specific domain*), and to build the corresponding mesh. When dealing with the simulation of many instances of a biophysical phenomenon (be it on many different patients, or for one patient at many different times), it is of paramount importance to have efficient algorithms for defining and meshing the domain. Motivated by this practical requirement, our study aims at defining a method that simultaneously provides the

[1] IMB, Université de Bordeaux, France
[2] IRMA, Université de Strasbourg, France
[3] Laboratoire IMATH (EA 2134), Université de Toulon, France
[4] CNR, IMATI "E. Magenes", Italy

geometry description and a mesh of good quality for the patient-specific domain, to be used for the simulation of a biophysical phenomenon (which reduces to solving a certain partial differential equation).

This step consists in identifying the different parts of the anatomy and in marking them with labels, thus resulting in the so-called "atlas". This registration step also yields a map from the atlas to the image to be segmented, providing an assignment of labels and segmentation that is *an inherited geometry description*.

Our approach exploits the features of *atlas-based segmentation*, a well-known technique [26] where the image is segmented by performing a registration with a pre-segmented, labeled image (the "atlas") that preserves the geometry and topology of the domains of interest, and represents the anatomical structure and their neighborhood relationships. Indeed, this segmentation yields, as a by-product, a map between the two images, which can be used to transfer additional data or information (in our case, a mesh). Given a reference (atlas) image, and a patient-specific image, the procedure consists in the following main steps (see Figure 1):

Step 1. Perform a segmentation of the reference (atlas) image, thus obtaining a model description of the geometry, and generate a mesh of the domain of interest. This reference mesh is called *atlas mesh*.

Step 2. Perform a co-registration of the patient-specific image with the reference atlas image, thus obtaining a transformation between the two images; in this way we transfer the segmentation to the new image (*atlas-based segmentation*)

Step 3. Using the transformation resulting from Step 2, the atlas mesh is deformed to fit the patient-specific domain, thus obtaining a new, patient-specific, mesh.

Since Step 1 and Step 2 are mutually independent, they can be done in parallel. Moreover, in case one needs to treat several patient images sharing the same reference atlas image, Step 1 is performed only once and for all.

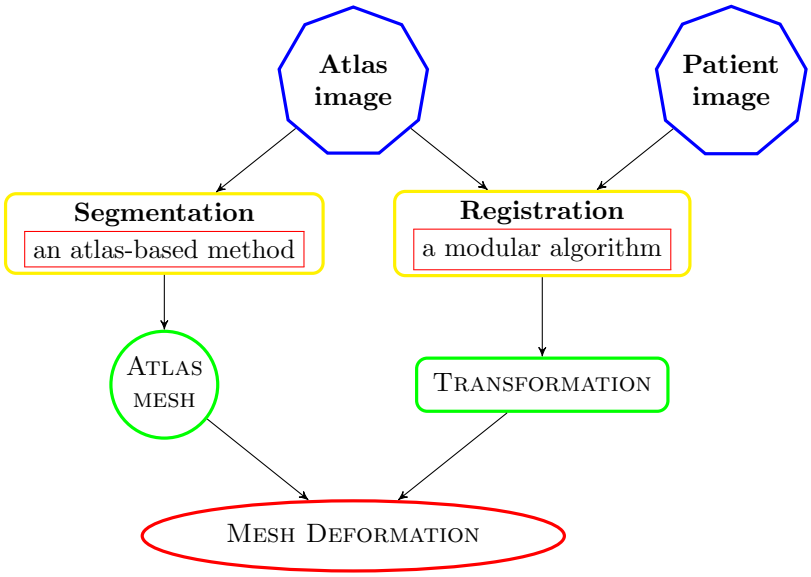

FIGURE 1. Sketch of mesh construction sheme.

The segmentation of the reference in Step 1 can be performed by any available segmentation technique (in our examples, it is performed "by hand").

The image registration procedure in Step 2 is carried out by resorting to the modular registration algorithm of S. Bertoluzza *et al.* [22], which splits the registration task in three mutually independent modules by tackling the three different ingredients involved in the registration procedure, namely

i) the computation of an image metric,

ii) the rules to carry out image interpolation, extrapolation and differentiation, and
iii) the definition of the chosen class of parametric image transformations.

The modular structure of the algorithm makes its usage flexible, allowing to independently develop and improve each of the three ingredients.

The paper is structured as follows: Sections 1 and 2 recall the atlas-based image segmentation method and the modular image registration algorithm, respectively. In Section 1, we detail the construction of atlas geometry description and meshes. In Section 2.4, we describe mesh deformations and the resulting creation of patient meshes. Section 3 is devoted to mesh quality analysis and to some simulations solving three model partial differential equations in the patient-related meshes. Section 4 concludes the paper and presents further works.

1. ATLAS-BASED SEGMENTATION

A monochromatic digital image can be modeled as a matrix (respectively a tensor, for three dimensional images) of the positive values, representing the brightness at the corresponding pixel (respectively voxel). Segmenting such an image consists in assigning a semantic label to each of its pixels (or voxels). There are different approaches to image segmentation, each requiring specific types of image information and constraints on the segmented geometry, and resulting in different methods and algorithms. Just to make some examples, let us mention purely intensity-based classification methods [20, 39, 42], level-set methods [23, 27, 36], snakes or active contours [43], atlas-based segmentation methods [2, 10, 15, 26]. The choice of a suitable method among all those available, relies on different considerations and depends, among other things, on the type of image data that one deals with, on the objects represented by the image, and on the desired output.

We are interested in medical images, such as MR images, CT scans or X-rays, with the main objective to retrieve, the geometrical description of an organ of interest (the "patient-specific domain"), and to build a mesh of such a domain in view of some kind of biophysical numerical simulations. Rather than dealing with a specific application, we aim at defining an application independent strategy for the construction of the patient-specific mesh needed for whatever application is at hand. Among different segmentation techniques, we focus our attention on the *atlas-based segmentation*, which takes advantage of the available a priori information on the spatial relation between the different components of the image (which, in our framework, correspond to different anatomical organs or portion of organs), and on their morphometric characteristics. By exploiting this information [18], which can include knowledge about the shape, orientation, continuity, and smoothness of the object to be segmented, atlas-based segmentation can be successful even in the absence of sharp boundaries, and can handle images with no well defined relations between regions and pixels intensities, a situation that can happen in the presence of noise, or when objects of the same texture need to be segmented.

Atlas-based segmentation, has, among other segmentation techniques, a further advantage: together with the segmented image, it provides a map that can be used to transfer any additional information from the reference image (the atlas) to the patient-specific image. In particular, it can be used to transfer to the patient-specific image, information such as a parametrization of the boundary of the domain of interest or the coordinates of the nodes of a finite element mesh for the numerical simulation.

1.1. Atlas and atlas mesh

While our algorithm deals with digital (discrete) images, it is convenient to look at digital images as discrete approximations of continuous images. This allow us to compare images at different resolutions, and give a natural meaning to mathematical objects such as the gradient of an image. In order to mathematically model the atlas-based segmentation method, let us introduce the following definition, where we normalize images to take values in $[0, 1]$ and where 0 corresponds to black and 1 to white.

Definition 1.1.

(a) A monochromatic (grey) image is a real valued function $R : \Omega \to [0, 1]$ where Ω is a subset of $\mathbb{R}^d$, $d = 2, 3$. Ω is called the domain of image R.

(b) Given a finite label set $L = \{e_1, e_2, ..., e_K\}$, a labeling map $A : \Omega \to L$ is said to be an *atlas*.
(c) A monocromatic *atlas image* is a couple (R, A), where R is a monochromatic image and A is an atlas.

Observe that the superposition of A and R yields a segmentation of A into structures identified by the labels of the label set L. Then, an atlas is a segmented image, where different regions, corresponding to the different labels, can be identified. For the atlas to be meaningful, the labeled region must correspond to the different structures represented in the image.

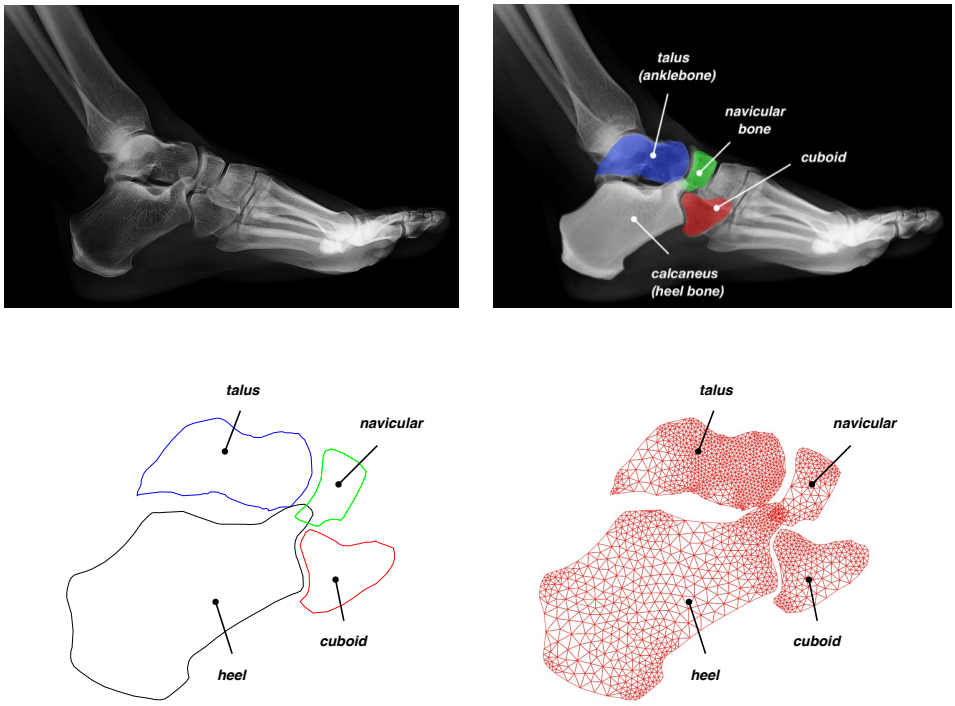

FIGURE 2. Atlas image of a foot with a classification of bones and a description of the geometry shape of each bone considered. The fourth subfigure shows the meshes built on the atlas image. These meshes are consequently associated with the labels: heel, talus, navicular and cuboid.

In the domain Ω of the image, we can identify specific subdomains as counterimages of the different labels in L. For each of these subdomains, we can then define an *atlas mesh*, defined as a conforming decomposition of the subdomain into the non overlapping union of triangles or quadrangles (in 3D, of tetrahedra or hexahedra).

The atlas image and mesh can be obtained from a given reference medical image through the following steps:

(1) segment the medical image thus defining the contours of the regions of interest;
(2) assign the corresponding labels to pixels belonging to the regions of interest, thus creating the atlas;
(3) retrieve a set of sample points on the contours of the subdomains identified by the different labels;
(4) generate the mesh from sample points on the boundaries.

Steps (1) and (2) can be performed by any available mean.We recall that the definition of the atlas is itself an interesting problem, and we refer to [26] for more details. In this paper, the segmentation and labeling of the image are performed by hand using an image editing tool and the contours of the region of interest are then retrieved by applying a level set method. Step (3) is more delicate since a sufficient number of sample points on the contour needs to be retrieved in order to ensure a sufficiently good approximation of the (a priori curved) geometry of the region of interest. Moreover, the density of sample points directly affects the quality of the

mesh, for instance, in the corners of specific domains. There are several available techniques for smoothing the contours (with convolution) and quantifying sample points with respect to approximative curvature. Step (4) is the heaviest step, however, many mesh generators can be found in the literature and, here, we rely on the Delaunay algorithm [11].

In Figure 2, we describe the four steps of meshing a medical image of a right foot. The geometry description of the atlas is made up of the four interested bones: calcaneus, cuboid, navicular and talus. The use of atlas-based segmentation allows us to deal with situations where multiple labels are assigned to the same pixel and this represents a further advantage of this segmentation technique (in the present example we observe a superposition between talus, calcaneus and navicular).

2. From the atlas mesh to the patient-specific mesh

As mentioned in the introduction, the atlas-based approach reduces the image segmentation problem to an image registration problem. Denoting by **Im** the space of monochromatic (continuous) images (Definition 1.1), let $R : \Omega \to \mathbb{R}^+$, $T : \Omega \to \mathbb{R}^+$ be two images in **Im**, which we assume for simplicity defined over the same domain Ω. Registering (or coregistering) the two images means finding, in a given class $\mathcal{T}$ of admissible transformations, a mapping $\theta : \Omega \to \Omega$ such that $T \circ \theta$ and R are as *"close"* as possible, as measured by a given "distance" functional $d : \mathbf{Im} \times \mathbf{Im} \to \mathbb{R}$. In other words, the registration of R and T reduces to the following optimization problem:

$$\text{minimize, over } \mathcal{T}, \text{ the functional} \quad \theta \mapsto d(R, T \circ \theta).$$

The choice of the "distance" functional d and of the class of admissible transformations $\mathcal{T}$ depends on the user's purpose. For both components, many choices have been studied in the literature, going from the simplest (least squares distance and rigid transformations) to more sofisticated ones [35]. Different choices will lead to different minima, and, consequently to different solutions to the image registration problem. Since in practice we deal with discrete digital images rather than with continuous images, the registration algorithm is also affected by how the discrete data of the pixel values is interpreted, which will lead to different recipes for evaluating quantities such as the point value of an image, or its differential.

In this paper, we restrict ourselves to classes of (non rigid) parametric transformations. For $\bar{\Omega} \in \mathbb{R}^d$, $N = 2, 3$, let us consider a finite dimensional linear subspace of $C^2(\overline{\Omega})$ spanned by a basis $\{\varphi_1(x), \varphi_2(x), ..., \varphi_M(x)\}$. We denote by $\mathcal{T}$ the class of parametric transformations consisting of all the mappings $\theta_\alpha : \bar{\Omega} \to \mathbb{R}^d$ of the form

$$\theta_\alpha(x) := x + \Theta(x; \alpha) \tag{1}$$

where, for a parameter vector $\alpha = (\alpha_k^i)_{k,i} \in (\mathbb{R}^M)^d \simeq \mathbb{R}^{Md}$, $\Theta(x; \alpha) \in (C^2(\overline{\Omega}))^d$ is given by

$$\Theta(x; \alpha) = (\Theta_i(x; \alpha))_i, \qquad \text{with } \Theta_i(x; \alpha) := \sum_{k=1}^{M} \alpha_k^i \varphi_k(x). \tag{2}$$

Since the range of $\Theta(\cdot; \alpha)$ is generally not a subset of Ω, to give a meaning to $T \circ \theta_\alpha$, we need to evaluate T also outside of Ω. Then we need to introduce an *extension operator* $\mathcal{E} : \mathbf{Im} \to L^\infty(\mathbb{R}^d)$ and the optimization problem can then be rewritten as

$$\alpha_{opt} = \arg \min_{\alpha \in \mathbb{R}^{NM}} c(\alpha), \qquad \text{with } c(\alpha) := d(R, \mathcal{E}T \circ \theta_\alpha). \tag{3}$$

Problem (3) is a nonlinear, unconstrained problem in $\mathbb{R}^{NM}$ and, to attain a global minimizer instead of local ones, we have to choose an appropriate method. We observe that even in the case that the selected image distance functional d is convex, the cost function c is not *a priori* a convex function of the unknown α. While

locally convergent algorithms like Newton's method and its variants (e.g. Gauss-Newton method and Inexact Gauss Newton method) are usually simple to be implemented and computationally competitive, whenever the initial point α_0 is sufficiently close to some minimizer [19, 25], in our context globally convergent methods, such as steepest descent methods, line search methods, trust-region methods, conjugate-gradient methods, quasi-Newton methods (see [25]), have to be preferred. In our tests we rely on the trust region method, as implemented in the Octave function `fminunc`.

Solving (3) by any gradient-based optimization method requires the (explicit) computation of the gradient of the cost function. In our case, the chain rule gives the following expression for the gradient of $c(\alpha)$:

$$\nabla c(\alpha) = \int_\Omega D\delta(\mathcal{E}T \circ \theta_\alpha; x)\ \nabla \mathcal{E}T(\theta_\alpha(x))\ J_\alpha\Theta(x;\alpha)\ dx, \tag{4}$$

where $\delta(\mathcal{E}T \circ \theta_\alpha; x) := d(R, \mathcal{E}T \circ \theta_\alpha)$, $\nabla\mathcal{E}T(\theta_\alpha(x))$ is the gradient of the (continuous) extended image $\mathcal{E}T$, and $J_\alpha\Theta(x;\alpha)$ is the Jacobian of the transformation Θ with respect to parameter α. The structure for ∇c given by formula (4) leads to the design of a modular toolbox code with the three following mutually independent modules:

$$\text{Distance module} + \text{Image module} + \text{Transformation module} \tag{5}$$

dealing respectively with the task related to the distance functional, the extension and differentiation of the image, and the application of the transformation and its Jacobian. Briefly, the distance module must provide the evaluation of the image distance and the computation of the gradient of the selected distance. The image module comprises an image extrapolation and interpolation model on which the corresponding image gradient will be processed. The transformation module is devoted to deforming the images and computing the Jacobian of the related deformation. For more details on the construction of this modular image registration algorithm, we refer to [22]. This modular structure facilitates not only the construction of the toolbox code but also its extension and use. Indeed, users can easily extend it by implement any image distance, as well as their own image differentiation scheme, and choose their favorite class of transformation, by simply locally modifying the corresponding module.

The main contribution to the computational cost of the proposed method comes from solving the nonlinear optimization problem (3). In order to make this step cheaper, a multiscale technique can be applied [3, 35], which speeds up the convergence of the co-registration procedure (3) by starting the optimization on lower resolution versions of the images to find a good enough transformation, and then by restarting the process within higher resolution.

In our implementation, we use the image registration toolbox presented in [22] which is equipped with several options of different image distances (including the well-known distances listed in Section 2.2) and image interpolation models. In the following we provide a description of the choices made within the different modules.

2.1. **The transformations class**

Different choices for the transformation class have been considered in the literature, including rigid transformations (translations, rotations), affine transformations, as well as more general non-rigid transformations (parametric [34], splines [7], B-splines [33, 35, 37, 38], thin plate splines [8]). Assuming, for simplicity, that $\Omega = [0,1]^d$, we look here for a deformation in the class of *interpolating scaling functions*. More precisely, we assume that $\Theta_i(x;\alpha)$, belongs to the d dimensional space obtained by tensor products starting from the one dimensional space of interpolating scaling functions on the interval constructed in [14] (see also [4, 5]). We recall that such a space is generated by the dilations and translations of the Daslaurier-Dubuc scaling functions (which are the autocorrelation functions of the Daubechies scaling functions), after suitable modifications at the boundaries.

Note that $\nabla_\alpha\vartheta(x;\alpha)$ depends on x but is independent of α. This is an immediate consequence of the linearity of the expansion (2) in the parameter and holds for any choice of the basis for the transformation space considered. Then $\nabla_\alpha\vartheta(x;\alpha)$ can be computed once and for all at the points of the grid matrix $\mathcal{G}$ (see Section 2.3).

2.2. The image distance

The role of the functional d is to measure the discrepancy between the two images. In the literature, there are numerous functionals for this purpose (or the equivalent purpose of measuring the similiarity between the two images). Even though such functionals are usually referred to as *image metrics*, most of them is not a metric in the mathematical sense of the term.

We choose the least square (LS) distance, which is the natural distance induced by the continuous image framework based on L^2-norm. More precisely, for any two images R, R' defined on the same domain Ω, the LS distance is given by

$$LS(R, R') = \frac{1}{2}\|R - R'\|^2_{L^2(\Omega)} := \frac{1}{2}\int_\Omega |R(x) - R'(x)|^2 dx.$$

Many other functionals can be used as a tool for measuring the "closeness" of the reference image and of the deformed template; among them we recall the normalized root least squares, the structural similarity index (SSIM, [9, 41]), which independently measures the similarity of luminance, contrast and structure, the Human visual system distance (HVS) [24] (a Fourier weighted L^2 distance with weight suitably defined in order to mimic the response of the human eye), the wavelet normalized root mean square error (WNRMSE) [1], and the mutual information [35].

2.3. The image model

We recall that both the reference image R and the template image T, in their digital form, are represented as d-dimensional arrays that we interpret as the average of the continuous images over each pixel/voxel. For simplicity we consider the same mesh size in all directions, which corresponds to a square or cubic image domain and to a square or cubic pixels. Then we consider digital images with a $N \times N$ or $N \times N \times N$ resolution. We let $h = 1/N$ and we set

$$\mathcal{G} = \{x^k = ((k_1 - .5)h, \cdots, (k_d - .5)h),\ k = (k_1, \cdots, k_d) \in \{1, \cdots, N\}^d\}.$$

We denote by pix_k the corresponding pixels

$$\mathrm{pix}_k = [hk_1, h(k_1 + 1)] \times \cdots \times [hk_d, h(k_d + 1)],\ k = (k_1, \cdots, k_d) \in \{1, \cdots, N\}^d\}.$$

In order to compute the cost function $c(\alpha)$ we need to sample the transformed image $\hat{T} = \mathcal{E}T \circ \theta$, with θ any admissible transformation at the points of the grid Ω_N or to compute its average at the corresponding pixel. Then, we have to evaluate the average of $\mathcal{E}T \circ \theta$ over the pixels. Applying the simplest one point quadrature rule (which is the choice that we made) reduces to approximating the average over a pixel with the value of $T \circ \theta$ at the center x^k of the pixel itself.

We then need to define the extension operator $\mathcal{E}$, allowing us to compute the values of T outside of its domain of definition. Our choice is to use a periodicity condition. Assuming that $\Omega = [0, 1]^2$, we set $\mathcal{E}T(x) = T(x - \lfloor x \rfloor)$. This introduces an artificial steep gradient at the boundary of Ω, whenever T does not actually satisfy periodic boundary conditions. First we note that many of the images in medical applications do actually satisfy periodic boundary conditions, since the image edges only see the background that is usually uniform. Secondly, numerical tests on generic images show that with a treatment of the gradient compatible with the periodic boundary conditions (i.e., if the steep gradient at the boundary induced by the periodic boundary conditions is indeed correctly computed), this artifact does not hinder the registration algorithms.

We also need to evaluate T at the points $\theta(x_k)$. The simplest way of doing this would be to identify the pixel to which $y_k = \theta(x_k)$ belongs, and use the corresponding value of the digital image. However, this *nearest neighbour approach* results in modeling the image as a piecewise constant, which is not differentiable. Instead, our approach to evaluating T at a generic point $y \in \Omega$ consists of perfoming a d-cubic interpolation based on a centered stencil, whose points are the centers of the pixels, i.e. the values at points outside Ω is defined by periodicity, according to the definition of the extension operator $\mathcal{E}$.

The second problem is the computation of the gradient of T at the points of the deformed grid, which we address by performing a second order centered scheme on a refined version of the image obtained by iteratively applying L times the above mentioned N-cubic interpolation.

Remark 2.1. Since we deal with digital images, where high frequency information has been discarded, we can always assume that the original analog image has the needed degree of regularity. However, we need to choose the reconstruction procedure, so that the L^∞ function that we would obtain by reconstructing T at all points of Ω exhibits a sufficient degree of smoothness (C^2 is needed for most optimization algorithms).

2.4. **Definition of the patient-specific mesh**

Let us now come to the main problem of defining a patient-specific mesh. More precisely, let T be a patient-specific image, defined on Ω, and let $\Omega_0 \subset \Omega$ be the subdomain corresponding to the anatomical structure that we need to mesh, in order to perform some numerical simulation. The standard approach consists in applying some segmentation procedure to T, to single out the subdomain Ω_0, and then in using a meshing procedure to the latter. If the same problem has to be solved for many different patient-specific geometries, obtained from different images (e.g. when repeating the same simulation on many different patients, or at many different times for the same patient), both the segmentation and the meshing procedures will be repeated several times. The main idea of this paper stems from the observation that, in addition to the segmentation of the image at hand, atlas-based segmentation yields, the transformation θ_α (in our case of the form (2)), such that the deformed image $R' = \mathcal{E}T \circ \theta_\alpha$ is (ideally) exactly superposed to the reference image R. The patient-specific anatomical structure Ω_0 is then defined as the deformation of the corresponding template anatomical structure $\widehat{\Omega}_0$ (generally defined as $\widehat{\Omega}_0 = \{x \in \Omega : A(x) = e\}$ with $e \in L$ one of the labels). If we have a mesh $\widehat{\mathcal{M}_h}$ on $\widehat{\Omega}_0$, we easily define a mesh on Ω by simply applying θ_α to the coordinates of the nodes of $\widehat{\mathcal{M}_h}$ and keeping the connectivity as it is, which, once θ_α is computed, makes the actual computation of the new mesh extremely cheap).

Notice that when the patient-specific domain is a non connected domain with different components, corresponding to different anatomical structures, then each component of the atlas mesh can be deformed, either separately or at the same time (depending on the user's goal), by the same transformation θ_α that can be computed only once. Form the practical point of view, these sub-steps will be facilitated by recording θ_α for reusing.

2.5. **"A priori" vs "a posteriori" adaptivity**

An important goal of our work is to reduce, as far as possible, the computational effort involved in the numerical simulation of biophysical phaenomena, while preserving the good quality of the solution of the problem at hand, solved on several similar geometries. An important ingredient to reach this goal is the use of adaptivity, and the standard approach would be to apply an adaptive procedure to each patient-specific problem, independently. However, in many situations the different patient-specific problems are qualitatively similar. This leads us to consider an alternative option, namely to build a non uniform "adapted" version of the atlas mesh and transfer it to the patient-specific domain through the transformation θ_α. The idea is to run an adaptive procedure on a "reference" problem, posed on the subdomain $\widehat{\Omega}_0$ derived from the reference image R.

Assuming that we need to solve several instances of patient-specific problems, we represent them in abstract form as

$$\mathcal{A}(u; \Omega_0, \mu) = 0$$

defined on the patient-specific domain $\Omega_0 \subset \Omega$ and possibly depending on a vector μ of patient-specific parameters. The idea is to consider a problem

$$\mathcal{A}(\widehat{u}; \widehat{\Omega}_0, \widehat{\mu}) = 0,$$

where $\widehat{\Omega}_0$ is the reference anatomical structure and $\widehat{\mu}$ is a suitably selected reference value for the parameter vector μ. We can then run an adaptive solver and retrieve the adapted mesh that can be transfered to different

patient-specific domains through the transformations θ_α stemming from the atlas segmentation procedure. Figure 3 compares the standard approach (DA) to this new approach, (AD). In many cases (when the singularity of the solution stem from shared geometrical or physiological features), this mesh (which, when considering the patient-specific problem, has been adapted "a priori"), will be enough. In other cases, it will provide a good starting point for a (patient-specific) standard adaptive procedure.

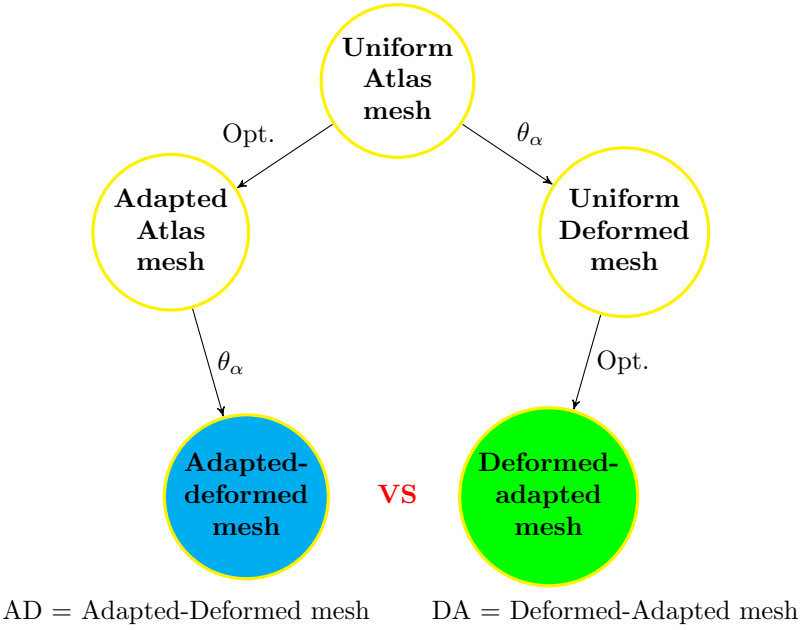

FIGURE 3. What is the optimized scheme for mesh construction ?

3. NUMERICAL TESTS

For all tests in the present paper, we used stock images that we acquired online[1].

3.1. **Test One**

First we test our method on a toy example, see Figure 4. We start from the reference image, the x-ray of a knee, and we construct the "patient-specific" knee image T, by manually deforming R in a smooth way, using a mainstream commercial image processing software. We build an atlas on the reference image and we use the transformation obtained from the co-registration between the atlas image and the patient image to deform the atlas meshes to fit the patient-specific domain.

[1] ©{MonthianRitchan-ad,kravka,andesign1010}@123rf.com

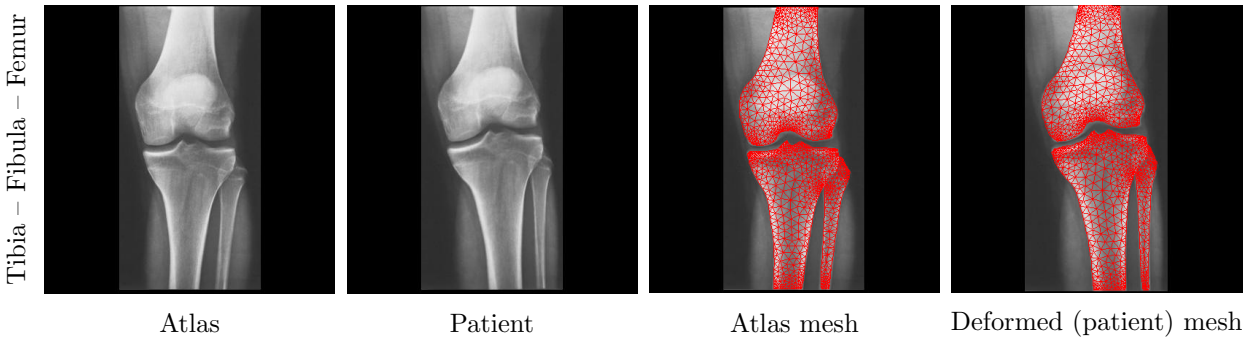

FIGURE 4. Atlas and patient images of an arm and a knee. Atlas meshes are deformed to fit the patient-specific domain.

3.2. **Test Two**

The second test is more challenging, as T and R are now two different, independently acquired, stock images of a lateral x-ray of a foot, for which we do not have, a priori, the existence of a transformation that allows the exact superposition of the two. Nevertheless, the registration procedure is able to achieve an excellent superposition of the calcaneus bone.

Figure 5 shows the result of the registration procedure. We display the image R (Atlas), the image T (patient) and the superposition of R and $T \circ \theta_\alpha$ (obtained as an RGB color image where the R (resp. G) color band contains the grey levels of the monochromatic image R (resp. $T \circ \theta_\alpha$). Figure 6 shows the atlas mesh and the patient mesh obtained by transforming the atlas mesh. Observe that, while the heel, cuboid and navicular are meshed in an acceptable way, the same does not hold for the talus. This is due to the significantly different shape that such a bone has in the two images. The transformation class used in the test does not allow us to compensate for such a difference, while retaining the good representation of the other three bones. We believe that this problem can be overcome by locally enhancing the transformation class (e.g. by exploiting the intrinsic multilevel nature of interpolating scaling functions), or by giving more weight (in the registration procedure) to the region of interest.

(A) Atlas (B) Patient (C) Transformed image

FIGURE 5. Single scale transformation with 512×512 resolution.

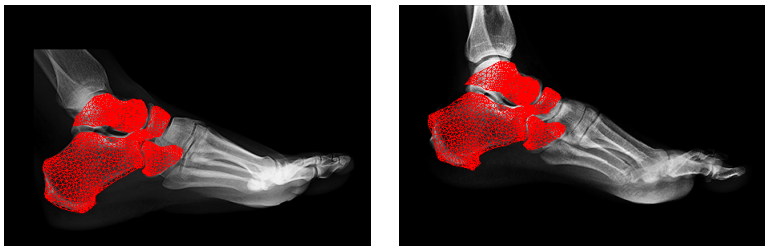

(A) Atlas (B) Patient

FIGURE 6. The atlas mesh and the patient-specific mesh

3.3. **Test three – "A priori" and "a posteriori" adaptivity**

We now test the effectiveness of the "a priori" computation of an adapted mesh, performed according to the idea presented in Section 2.5. We consider three simple equations:

3.3.1. *Poisson equation*

$$\begin{cases} -\Delta u = 10^{-2} & \text{in } \Omega_0 \\ u = 0 & \text{on } \partial\Omega_0. \end{cases} \tag{6}$$

3.3.2. *Elastic equation*

$$\begin{cases} -\nabla \cdot \boldsymbol{\varepsilon}(\boldsymbol{u}) = \rho \boldsymbol{g} & \text{in } \Omega_0 \\ \boldsymbol{u} = \boldsymbol{0} & \text{on } \partial\Omega_0 \end{cases} \tag{7}$$

where $E = 14.8\ 10^6$ Pa, $\nu = 0.19$, and $\rho = 1.9\ 10^3$ kg m^{-2}.

3.3.3. *Advection-Diffusion-Reaction equation*

$$\begin{cases} -k\Delta u + \boldsymbol{\beta} \cdot \nabla u + u = f & \text{in } \Omega_0 \\ u = u_{ex} & \text{on } \partial\Omega_0 \end{cases} \tag{8}$$

where $k = 10^{-5}$, $\boldsymbol{\beta} = [0\ 1]^T$, and $u_{ex} = kxy^2$.

These equations are solved on a toy patient-specific domain Ω_0 obtained by the Tibia-fibula image of Figure 4. For the sake of simplicity, the patient-specific domain is supposed to be simply connected. Observe that the domain is not anatomically correct, as it merges in a single domain the two independent bones. However, as we are not interested in a specific medical application but rather in demonstrating the feasibility of a general meshing strategy, the tests that we are going to perform are still significant. We emphasize that the domain Ω_0 is not trivial since, as we observe in Figure 7, its boundary has curvatures positive and negative. In particular, it presents sharp corners that affect the quality of the mesh and thus the mesh where the partial differential equations is solved. We show in Figure 7 the non optimized meshes of the atlas (reference) and patient domains.

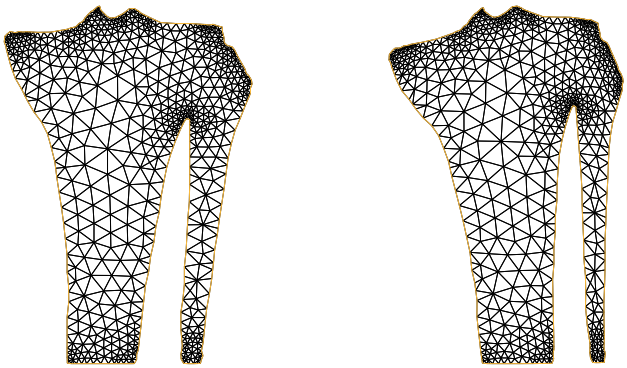

Atlas mesh Patient mesh

FIGURE 7. Non optimized meshes.

In order to perform the mesh adaptation, both on the reference problem for the "a priori" adaptive mesh computation, and, for comparison, on the patient-specific problem, we used the MATLAB command `adaptmesh` which, given an initial mesh, iteratively generates a sequence of solutions computed on iteratively refined meshes. The refinement is based on standard element-wise error indicators $E(K)$,([16, 17]), which, for the generic diffusion-reaction $-\nabla \cdot (\mu \nabla u) + \gamma u) = f$ takes the form

$$E(K) = \alpha \|h(f - \gamma u)\|_{L^2(K)} + \frac{\beta}{4} \left(\sum_{\tau \in \partial K} h_\tau^2 \mu^2 \left[\frac{\partial u_h}{\partial n_\tau} \right]^2 \right)^{1/2}.$$

Here, u_h is the piecewise linear discrete solution computed over the triangulation $\mathcal{T}_h$, $h = h(\boldsymbol{x})$, τ is an edge of K, and $\partial v / \partial n_\tau$ is the normal derivative of v along the edge τ. α and β are constants independent of the triangulation.

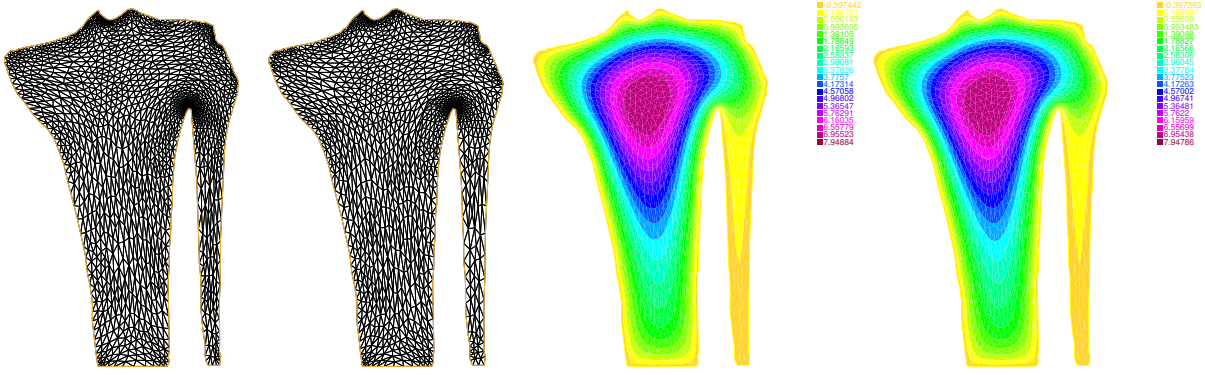

AD mesh DA mesh Sol. on AD mesh Sol. on DA mesh

FIGURE 8. Adapted meshes and solutions of the Poisson equation.

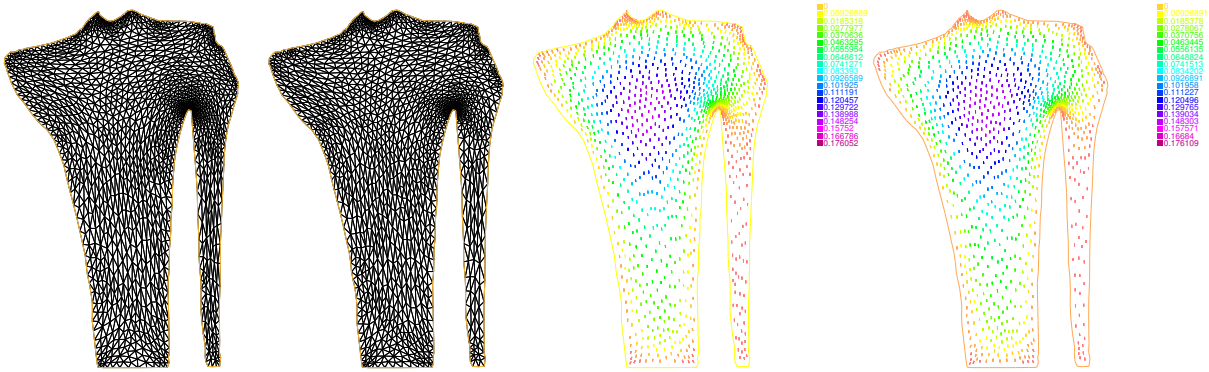

AD mesh DA mesh Sol. on AD mesh Sol. on DA mesh

FIGURE 9. Adapted meshes and solutions of the Elastic equation.

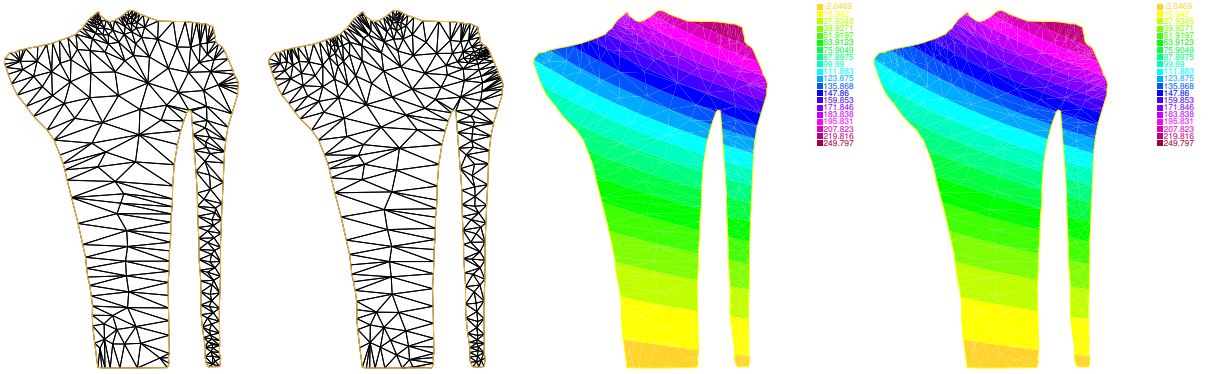

AD mesh DA mesh Sol. on AD mesh Sol. on DA mesh

FIGURE 10. Adapted meshes and solutions of the ADR equation.

3.3.4. *Comparison of the results*

In Figures 8, 9 and 10 we compare, for the three model problems, the meshes and the solutions obtained with the two approaches presented in Section 2.5 (resp. AD and DA). Observe that on the two isotropic problems the cheaper (if multiple instances of the same problem on geometries deriving from different images) AD strategy gives comparable results with those obtained by the standard DA strategy. For the advection-diffusion-reaction case, the results show a greater difference, due to the anisotropy of the problem.

We continue the comparison by reporting in Table 1, for the three problems and the two strategies, the attained relative error:

$$\text{Relative error} = \frac{\|u - u^*\|_{L^2(\Omega)}}{\|u^*\|_{L^2(\Omega)}}, \tag{9}$$

where u^* is either the exact solution or the best (reference) solution. The results confirm the observation of the previous sections. For Problems 6 and 7 the results obtained by the AD strategy are comparable to those obtained by the (standard) DA strategy. On the other hand, for Problem 8 we see an evident loss in the relative error when relying on the AD strategy, with respect to what we obtain by the widely accepted DA strategy.

Equation	AD	DA
Poisson	1.95 E-3	1.91 E-3
ADR	4.09 E-4	2.69 E-4
Elastic	2.44 E-3	2.48 E-3

TABLE 1. Relative estimates on adapted-deformed (AD) and deformed-adapted (DA) meshes.

4. Conclusion and perspectives

We presented a general strategy for defining the geometry and the mesh for patient-specific numerical simulation of biophysical phaenomena. The strategy is based on atlas-based image segmentation and consists in taking advantage of the transformation stemming from the image registration step of atlas-based segmentation, for transfering onto the patient-specific domain, geometry and mesh information pre-defined on the reference (atlas) domain.

The numerical tests performed, give a first confirmation of the feasibility of our strategy, while pointing out some of its limitations, thus suggesting several directions for future research aimed at understanding the field of potential application and at tackling its weaknesses.

Work needs to be put in understanding how to better capture the finest features of the geometry. This issue can be tackled from different sides such as the definition of the distance and the selection of the transformation class. However, it seems important to be able to perform some kind of refinement on the class of transformations. Here, the use of a class of transformation inherently endowed with a multilevel structure (such as the class of interpolating wavelet that we use here) seems quite promising.

Obviously, we would like the deformed mesh to inherit as much as possible the (good) shape regularity properties of the reference mesh. In order to attain this goal, it might be useful to include, in the cost functional, a term penalising the possible lack of smoothness of the transformation. We might for instance think of replacing the functional $c(\alpha)$ with

$$c_\lambda(\alpha) = c(\alpha) + \lambda \|\nabla \theta_\alpha\|_2^2,$$

or, more generally, with

$$\tilde{c}(\alpha) = d(T \circ \theta_\alpha, R) + E(\theta_\alpha)$$

where $E(\cdot)$ is some measure of distortion resulting from the transformation θ_α.

Since the algorithm that we relied on is structural, an extension for three dimensional image data should be straightforward. However, since the computation will require memory and CPU time, we plan to tackle this extension by using a high-performance computational platform.

References

[1] M.G. Albanesi, R. Amadeo, S. Bertoluzza, G. Maggi. *A new class of wavelet-based metrics for image similarity assessment.* Journal of Mathematical Imaging and Vision, Vol. 60, Issue 1, pp 109–127, 2018.

[2] C. Baillard, P. Hellier and C. Barillot. *Segmentation of brain 3D MR images using level sets and dense registration*, Medical Image Analysis, Vol. 5, No. 3, pp. 185–194, 2001.

[3] G. Maggi. *Registration algorithms for medical images.* Ph.D Thesis. 2013.

[4] S. Bertoluzza, G. Naldi. *A wavelet collocation method for the numerical solution of partial differential equations* . Appl. and Comput. Harm. Anal., Vol 3, pp. 1–9, 1996.

[5] S. Bertoluzza, V. Perrier. *A new construction of boundary interpolating wavelets for fourth order problems* . Acta Appl. Math., Vol152, pp. 33–56, 2017.

[6] O. V. Besov. *On a family of function spaces. embedding theorems and extensions.* Dokl. Acad. Nauk SSSR, Vol 126, pp. 1163–1165, 1959.

[7] P. Bézier. *Courbes et surfaces pour la CFAO*, Techniques de l'ingénieur Applications des mathématiques, No A1440, 1992.
[8] F. L. Bookstein. *Principal warps: Thin-plate splines and the decomposition of deformations*. IEEE Transactions on pattern analysis and machine intelligence, Vol 11, No 6, pp. 567–585, 1989.
[9] D. Brunet, E. R. Vrscay, Z. and Wang. *On the mathematical properties of the structural similarity index*. IEEE Transactions on Image Processing, Vol 21(4), pp. 1488–1499, 2012.
[10] D. L. Collins, C. J. Holmes, T. M. Peters and A. C. Evans. *Automatic 3D modelbased neuroanatomical segmentation*, Human Brain Mapping, Vol. 3, No. 3, pp. 190–208, 1995.
[11] B. Delaunay. *Sur la sphre vide. A la mmoire de Georges Voronoï*. Bulletin de l'Académie des Sciences de l'URSS, Classe des sciences mathématiques et naturelles, Issue 6, pp. 793–800, 1934.
[12] R. A. DeVore and V. A. Popov. *Interpolation of Besov spaces*, Transactions of the American Mathematical Society, Vol 305(1), pp. 397–414, 1988.
[13] R. A. DeVore and R. C. Sharpley. *Besov spaces on domains in ˆ{}*. Transactions of the American Mathematical Society, Vol 335(2), pp. 843–864, 1993.
[14] D. Donoho. Interpolating wavelet transform. 1992.
[15] J. C. Gee, M. Reivich and R. Bajcsy. *Elastically deforming a three-dimensional atlas to match anatomical brain images*, Journal of Computer Assisted Tomography, Vol. 17, No. 2, pp. 225–236, 1993.
[16] C. Johnson. *Numerical Solution of Partial Differential Equations by the Finite Element Method*. Lund, Sweden: Studentlitteratur, 1987.
[17] C. Johnson and K. Eriksson. *Adaptive Finite Element Methods for Parabolic Problems I: A Linear Model Problem*. SIAM J. Numer. Anal, 28, (1991), pp. 4377.
[18] H. Kalinić. *Atlas-based image segmentation: A Survey*. Department of Electronic Systems and Information Processing, Universiy of Zagreb. (2008)
[19] C. T. Kelley. *Iterative Methods for Linear and Nonlinear Equations*. SIAM, Philadelphia, 1995.
[20] N. Kovacevic, N. J. Lobaugh, M. J. Bronskill, B. Levine, A. Feinstein, and S. E. Black. *A robust method for extraction and automatic segmentation of brain images*, NeuroImage, Vol. 17, No. 3, pp. 1087–1100, 2002.
[21] P. G. Lemarié. *Some remarks on wavelet theory and interpolation*, Preprint, Mathématiques, Paris XI, Orsay, 1991.
[22] S. Bertoluzza, G. Maggi and S. Tomatis. *A modular registration algorithm for medical images*. International Conference Image Analysis and Recognition, Springer, pp 467–474, 2013.
[23] R. Malladi, J. A. Sethian and B. C. Vemuri. *Shape modeling with front propagation: A level set approach*, IEEE Transactions on Pattern Analysis and Machine Intelligence, Vol. 17, No. 2, pp. 158–175, 1995.
[24] J. L. Mannos and D. J. Sakrison. *The effects of a visual fidelity criterion on the encoding of images*. IEEE Transactions on Information Theory , Vol IT-20, pp. 525–536, 1974.
[25] J. Nocedal and S. Wright. *Numerical Optimization*. Springer-Verlag New York, 2006.
[26] T. Rohlfing, R. Brandt, R. Menzel, D.B. Russakoff, and C.R. Maurer, Jr., *Quo vadis, atlas-based segmentation* in Handbook of biomedical image analysis, Volume 3: Registration Models. Springer Science & Business Media, 2005.
[27] A. Sarti, C. O. De Solrzano, S. Locket and R. Malladi. *A geometric model for 3D confocal image analysis*, IEEE Transactions on Biomedical Engineering, Vol. 47, No. 12, pp. 1600–1609, 2000.
[28] Z. Shi and Z. Bao. *Fast image coding of interval interpolating wavelets*, Wavelet Application IV, SPIE, Vol. 3078, pp. 240–253, 1997.
[29] I. J. Shoenberg. *Cardinal Interpolation and spline functions: II. Interpolation of data of power growth*, Journ. Approx. Theory, Vol 6, pp. 404–420, 1972.
[30] J. S. Suri, D. L. Wilson and S. Laxminarayan. *Handbook of biomedical image analysis, Volume 1: Segmentation Models, Part A*. Springer Science & Business Media, 2005.
[31] J. S. Suri, D. L. Wilson and S. Laxminarayan. *Handbook of biomedical image analysis, Volume 2: Segmentation Models, Part B*. Springer Science & Business Media, 2005.
[32] J. S. Suri, D. L. Wilson and S. Laxminarayan. *Handbook of biomedical image analysis, Volume 3: Registration Models*. Springer Science & Business Media, 2005.
[33] P. Thévenaz, T. Blu, and M. Unser. *Interpolation revisited*. IEEE Transactions on Medical Imaging, 19(7), pp. 739–758, 2000.
[34] D. A. W. Thompson. *On Growth and Form*. Cambridge University Press. 1917.
[35] P. Thévenaz and M. Unser. *Optimization of mutual information for multiresolution image registration*. IEEE Transactions on Image Processing, 9(12), pp. 2083–2099, 2000.
[36] A. Tsai, Jr. A. Yezzi, W. Wells, C. Tempany, D. Tucker, A. Fan, W. E Grimson and A. Willsky. *A shape-based approach to the segmentation of medical imagery using level sets*, IEEE Transactions on Medical Imaging, Vol. 22, No. 2, pp. 137–154, 2003.
[37] M. Unser, A. Aldroubi, and M. Eden. *B-spline signal processing: Part I – theory*. IEEE Transactions on Signal Processing, 41(2), pp. 821–833, 1993.
[38] M. Unser, A. Aldroubi, and M. Eden. *B-spline signal processing: Part II – efficient design and applications*. IEEE Transactions on Signal Processing, 41(2), pp. 834–848, 1993.

[39] M. W. Vannier, T. K. Pilgram, C. M. Speidel, L. R. Neumann, D. L. Rickman and L. D. Schertz. *Validation of magnetic resonance imaging (MRI) multispectral tissue classification*, Computerized Medical Imaging and Graphics, Vol. 15, No. 4, pp. 217–223, 1991.

[40] P. Viola and W. M. Wells III. *Alignment by maximization of mutual information.* International journal of computer vision, Vol 24(2), pp. 137–154, 1997.

[41] Z. Wang, A. C. Bovik, H. R. Sheikh, and E. P. Simoncelli. *Image quality assessment: from error visibility to structural similarity.* IEEE Transactions on Image Processing, Vol 13 (4), PP. 600–612, 2004.

[42] W. M. Wells, W. E. L. Grimson, R. Kikinis and F. A. Jolesz. *Adaptive segmentation of MRI data*, IEEE Transactions on Medical Imaging, Vol. 15, No. 4, pp. 429–442, 1996.

[43] Jr., A. Yezzi, S. Kichenassamy, A. Kumar, P. Olver and A. Tannenbaum. *A geometric snake model for segmentation of medical imagery*, IEEE Transactions on Medical Imaging, Vol. 16, No. 2, pp. 199–209, 1997.